T. Makino et alii, Frattura ed Integrità Strutturale, 34 (2015) 334-340; DOI: 10.3221/IGF-ESIS.34.36

Focussed on Crack Paths

Effect of defect length on rolling contact fatigue crack propagation in high strength steel

T. Makino, Y. Neishi
Nippon Steel & Sumitomo Metal Corporation, Japan
makino.hb3.taizo@jp.nssmc.com, neishi.58e.yutaka@jp.nssmc.com

D. Shiozawa, S. Kikuchi, S. Okada
Kobe University, Japan
shiozawa@mech.kobe-u.ac.jp, kikuchi@mech.kobe-u.ac.jp

K. Kajiwara
Japan Synchrotron Radiation Research Institute, Japan
kajiwara@spring8.or.jp

Y. Nakai
Kobe University, Japan
nakai@mech.kobe-u.ac.jp

ABSTRACT. The objective of the present paper is to clarify the effect of defect length in depth direction on rolling contact fatigue (RCF) crack propagation in high strength steel. RCF test and synchrotron radiation micro computed tomography (SR micro CT) imaging were conducted. In the case of the defect with the 15 μm diameter, flaking life decreased with increasing defect length. In a comparison of the CT image and the SEM view, the shapes of defects and the locations of the horizontal cracks were almost the same respectively. The mechanism of RCF crack propagation was discussed by finite element (FE) analysis. Defects led to higher tensile residual stress than that without defects in the region where the defect exists. The shear stress range at 0.1 mm in depth on the middle line of the defect and the range of mode II stress intensity factor at the bottom of a vertical crack increased with increasing defect length.

KEYWORDS. Rolling contact fatigue; Artificial defect; Crack propagation; High strength steel; Synchrotron radiation micro computed tomography imaging; Stress intensity factor.

INTRODUCTION

Rolling contact fatigue (RCF) tests for evaluation of bearing steel are commonly conducted under pure rolling contact with oil lubrication. Non-metallic inclusions in internal region cause fatigue cracks [1-2]. Cracks propagate and eventually form typical RCF damage called flaking. The refinement of sphere-type inclusions like oxides has

been applied to increase flaking life. Recently it was indicated that stringer-type inclusions can be the origin of RCF cracks and flaking[3], and the inclusion length influenced the RCF life[4].
In the present paper, to discuss the mechanism of the above phenomena, RCF test was conducted using specimens with artificial defects that simulate stringer-type inclusions. The effect of defect length on flaking life was evaluated using specimens with different-length defects. Synchrotron radiation micro computed tomography (SR micro CT) imaging and microscope observation were performed for RCF cracks and their fracture surface. The morphology of RCF cracks before flaking was investigated. The experimental result was discussed in terms of stress states and fracture mechanics based on the analytical result by finite element (FE) analysis.

MATERIALS, SPECIMENS, AND TEST METHODS

Materials and specimens

Ball-on-disc type RCF tests were conducted under oil lubrication. Disc specimens were made of two steels: high carbon–chromium bearing steel JIS SUJ2 and induction-hardened 0.55% carbon steel JIS S55C. Both steels were received as rolled bars. SUJ2 bar was spheroidizing-annealed, and then quenched and tempered. S55C bar was normalized and was then machined to disc shape. The ring-shaped region of the ball rolling track surface was induction-hardened and tempered. The disc specimen was 60 mm in diameter and 5 mm in thickness. The diameter of ball rolling track was 38.5 mm, the region in the vicinity of the track had a Vicker's hardness of 700–750 HV in both specimens of SUJ2 and S55C. Artificial defects of 15 or 50 μm diameter and 30–300 μm length from surface in depth direction were introduced on the ball rolling track of the disc specimen by electro-discharge machining. The above length of defect is referred to as defect length in this paper. Ball specimens are commercial products made of SUJ2. The ball diameter was 9.525 mm.

Test methods

Three balls were rolled on one side of a disc specimen surface under oil lubrication. A vertical contact force was set so that the Hertzian stress p_{max} was 5.22 GPa. The half-width of the contact patch a was then calculated as 0.346 mm. Tests were continued until a preset number of cycles or automatically stopped by detecting the vibration due to flaking.

ROLLING CONTACT FATIGUE TEST RESULT

Fig. 1 presents the relationship between defect length and flaking life obtained from RCF test of SUJ2 disc specimen. In the case of the defect with the 15 μm diameter, flaking life decreased with increasing defect length. In the case of the defect with the 50 μm diameter, flaking life was almost constant from 50 to 300 μm of defect length and shorter than the shortest life in the case of the 15-μm-diameter defect.

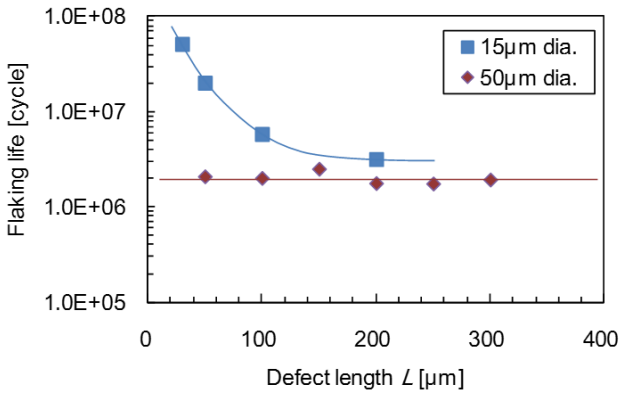

Figure 1: Relationship between defect length and flaking life obtained from RCF test of SUJ2.

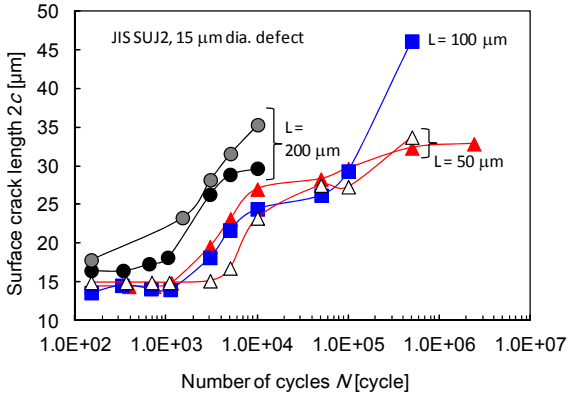

Figure 2: Changes in surface length of vertical crack including defect during RCF test.

Cracks were initiated at the edges of 15-μm-diameter defect in radial direction on rolling contact surface. According to the following investigation, they propagated not only in radial direction but also in depth direction along defect. These cracks are referred to as vertical cracks in this paper. The surface length of vertical crack including defect 2*c* was measured during RCF test. Fig. 2 shows changes in 2*c* during RCF test. Vertical cracks initiated at longer defects propagated faster.

SR MICRO CT IMAGING OF CRACK INITIATION AND PROPAGATION BEHAVIOUR

Inspection samples

In order to discuss the mechanism of the RCF damage described in the previous section, it is of great importance to clear how the cracks observed on surface propagate in internal region and form flaking. In this section, the morphology of internal cracks initiated in disc specimens of S55C inspected by SR micro CT imaging at SPring-8 is discussed. Artificial defects introduced in disc specimens were 15 μm in diameter and 50, 100, and 200 μm in defect length. The RCF test stopped at an arbitrary number of cycles. Inspection samples having a square cross section of 0.5 mm × 0.5 mm with the defect were taken from the disc specimens. The dimension is regulated by the penetrative thickness for the present X-ray energy for Fe material.

CT imaging method

CT imaging was performed at the BL19B2 beam line of SPring-8, the most powerful synchrotron radiation facility in Japan. The measurement conditions were as follows: X-ray energy of 37 keV and sample-detector distance of 0.7 m [5]. The effective pixel size of the detector was from 0.74 to 2.8 μm depending on the magnification of the beam monitor. For a 3-D reconstruction, a set of 900 radiographs of a sample were recorded at rotations over 180°, where each rotation angle was 0.2°. Slice images were reconstructed from the series of the projection images by a filtered-back projection algorithm.

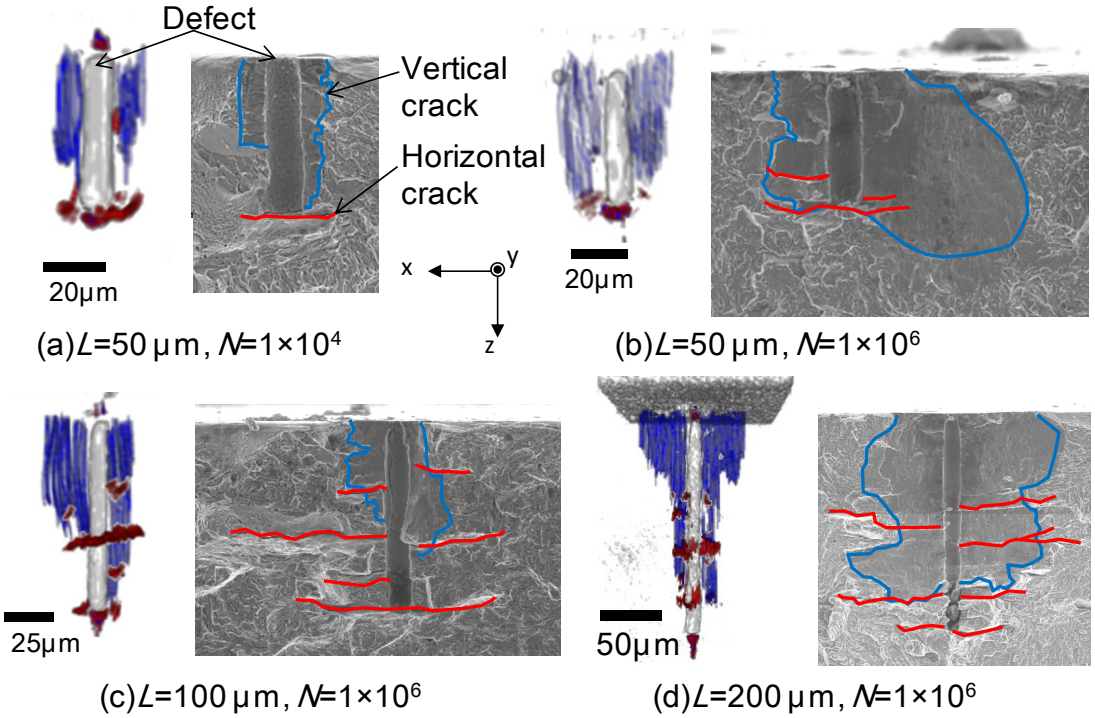

Figure 3: CT images and SEM view of artificial defect and cracks (Defect diameter: 15 μm, Left: CT image, and Right: SEM view).

CT Imaging result

Images of the artificial defect and cracks shown in the left-hand side of Fig. 3 were obtained by CT scanning. Several samples were broken at liquid nitrogen temperature to observe the fracture surface of the vertical crack. SEM views of the fracture surfaces are also shown in right-hand side of Fig. 3. Shapes of RCF cracks identified from fractography were also

indicated by lines on the SEM views of Fig. 3. Cracks parallel to the surface and perpendicular to the defect were observed. The cracks are referred to as horizontal crack in this paper. In a comparison of the CT image and the SEM view, the shapes of defects and the locations of the horizontal cracks were almost the same respectively, but the shapes of vertical cracks in CT images (Fig. 3 (b), (d)) were smaller in the deeper region than those in SEM views. These results provide the validity of CT imaging and future task for optimizing imaging condition.

Crack shapes and sizes between different number of cycles and defect lengths were compared from SEM views. Fig. 4 summarizes the comparison result in the same scale. A vertical crack initiated from a defect of 50μm length propagated in x and z (depth) direction from $N = 1\times10^4$ to 1×10^6. In comparison under the same cycles, horizontal cracks initiated from longer defects propagated longer.

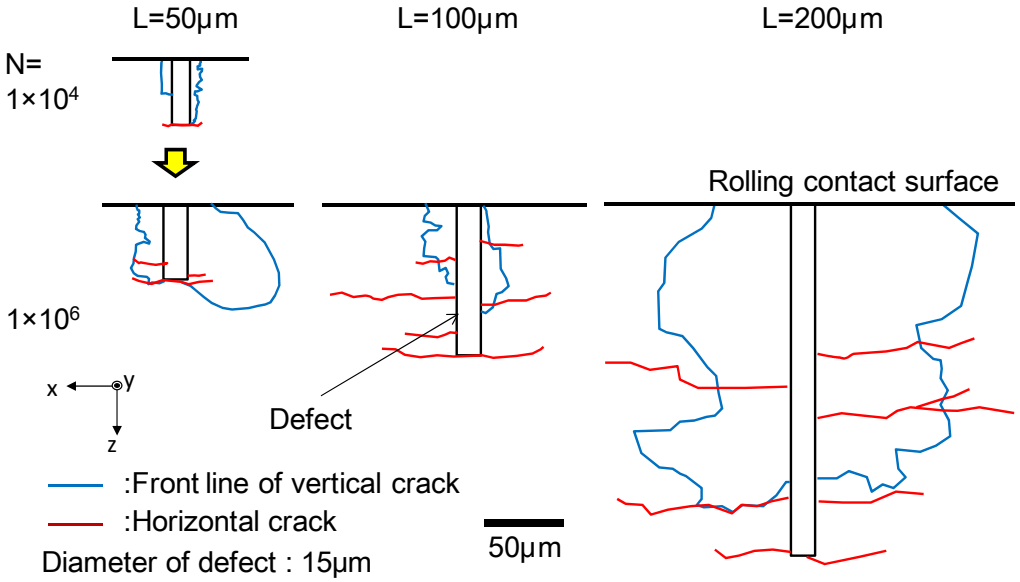

Figure 4: Comparison of crack shape and size between different number of cycles and defect lengths.

FINITE ELEMENT ANALYSIS OF STRESS STATES UNDER ROLLING CONTACT

FE analysis was conducted using models with a circular hole and/or a crack to evaluate the effect of defect length on the stress states around the defect and the stress intensity factors (SIFs) of the RCF cracks. ABAQUS Ver. 6.12 was used for the FE analysis.

FE modelling and analytical condition

A numerical FE model for the RCF test was developed as shown in Fig. 5. The FE model comprises a rectangular block for the disc specimen and a hemisphere for the ball specimen taking symmetry into account. A circular hole of the same size as the artificial defect, whose diameter was 15 μm, in the experiment was modeled in a small rectangular section. The section was tied at the centre of the disc specimen model. Models are classified into three types (i.e., defect without crack, vertical crack without defect, and defect and vertical crack; Fig. 5(b–d)). The defect model (Fig. 5(b)) comprises a hole with depth $L = 0$ (plane, no defect), 50, 100, 150, and 200 μm. The vertical crack model (Fig. 5(c)) comprises a vertical crack with the surface half length c of 15 μm and depth of 50 μm. The crack size was determined from the CT imaging result. The defect and vertical crack model (Fig. 5(d)) comprises a hole with the various depths mentioned above and a vertical crack with the above size. A fine mesh was applied to the region around the crack tip; the minimum length between nodes was 0.0005 mm at crack tip and 0.00125 mm on the internal surface of the hole. The number of elements was 242,093 and 32,914 in the rectangular model and hemisphere model, respectively.

Friction coefficients between the ball and disc specimen model and between crack faces were zero with the consideration of the oil lubrication. The elastic modulus and Poisson's ratio were 205.8 GPa and 0.3, respectively. In the case of elastic–plastic FE analysis, an experimentally measured stress–strain curve was applied in the disc specimen model. A vertical force was applied to obtain the same Hertzian stress p_{max} (5.22 GPa) as the experiment, then the half-width of the contact

patch a was 0.346 mm. The ball specimen model moved 8 mm across the circular hole and cracks on the disc specimen model along the symmetric surface. In the case of elastic-plastic analysis, stress states after four repeats of above cycle were evaluated.

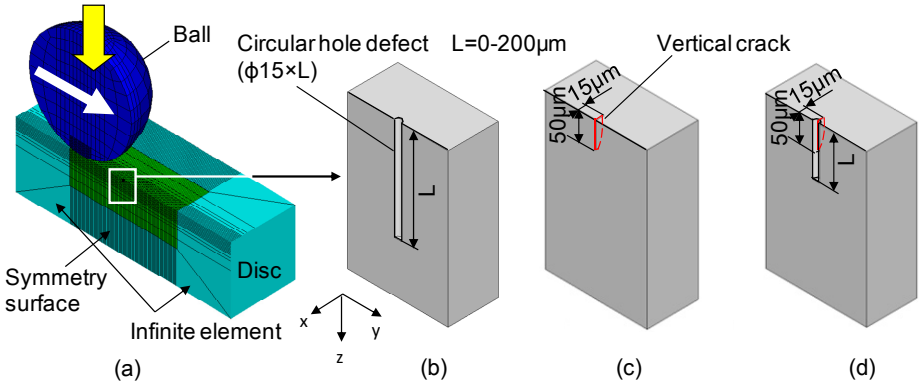

Figure 5: FE models for the RCF test. (a) Entire model. (b) Magnification of defect (without crack). (c) Vertical crack (L=0 μm). (d) Defect & vertical crack.

FE analysis result

In order to clarify the stress state at the artificial defect with different defect length during the passage of ball before crack initiation, the defect model shown in Fig. 5(b) was calculated by elastic–plastic FE analysis. Fig. 6 shows the residual stress in y-direction distributions on the middle line of the hole (in z-direction). Remarkably high tensile residual stress was generated at the surface edge of the defect. The residual stress distribution exhibited a peak value below the surface and a decrease from the depth of the peak to the bottom of the defect. Furthermore, it shifted to the distribution of residual stress, which was in compression side, in the plane model (L = 0 μm, without defect). Defects led to higher residual stress to tension side than that without defects in the region where the defect exists. Fig. 7 presents the variation in shear stress τ_{yz} at 0.1 mm in depth on the middle line of the hole during rolling contact obtained from elastic-plastic FE analyses. The shear stress had a peak and a valley before and after rolling contact. The shear stress range, derived from the peak and the valley of the shear stress, was the smallest in the case without defect, larger in the case of L = 100 μm (L coincides with the stress evaluation point), and the largest in the cases of L = 150 and 200 μm.

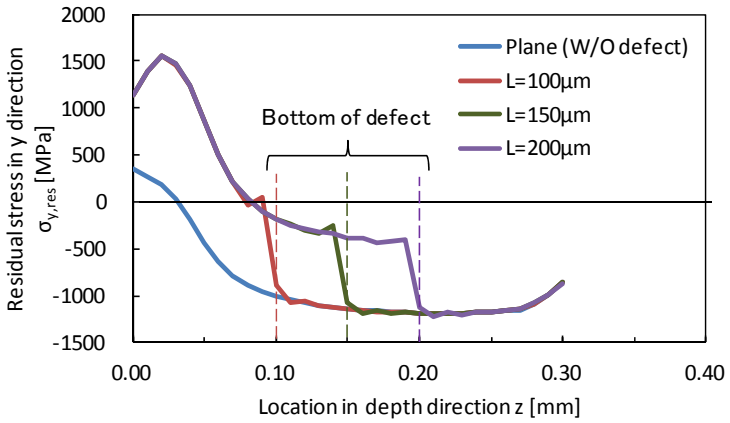

Figure 6: Residual stress distributions along defect obtained from elastic–plastic FE analyses.

SIFs for vertical cracks with and without defects were evaluated from elastic FE analysis. The size of the crack was constant, but the defect length (hole depth in the model) L varied from 0 to 200 μm. The mode I SIF K_I at the surface edge of vertical crack and the mode II SIF K_{II} at the bottom of vertical crack were calculated from the displacement distribution on the crack face near the crack tip. The ranges of SIF ΔK_I and ΔK_{II} were derived from the variation in K_I and K_{II} respectively during rolling contact. ΔK_I (V-S) and ΔK_{II} (V-B) were compared between different defect lengths in Fig. 8.

ΔK_{II} increased with increasing L, but ΔK_I slightly decreased simultaneously. A case of L = 50 μm implies that the vertical crack tip reaches the bottom of the defect. On the other hand, a case of L > 50 μm implies that the vertical crack tip is before reaching the bottom of the defect. ΔK_{II} at L = 50 μm was larger than that at L = 100 μm. This result suggests that when the vertical crack tip reaches the bottom of the defect, the increase of ΔK_{II} due to crack propagation exhibits slowdown or decrease; the propagation of the vertical crack is retarded.

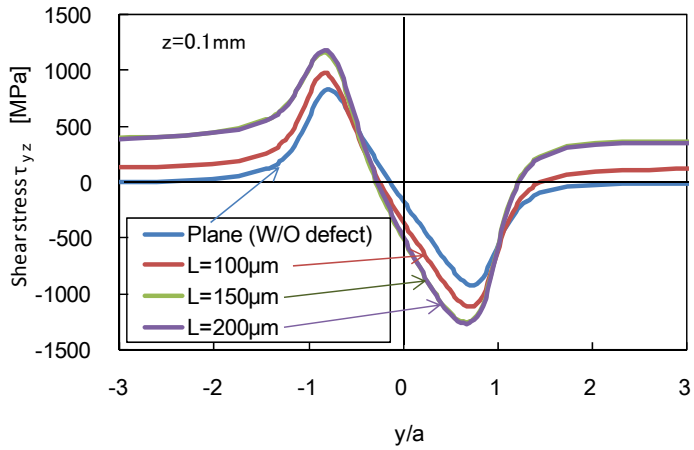

Figure 7: Variation in shear stress at 0.1 mm depth during rolling contact obtained from elastic–plastic FE analyses.

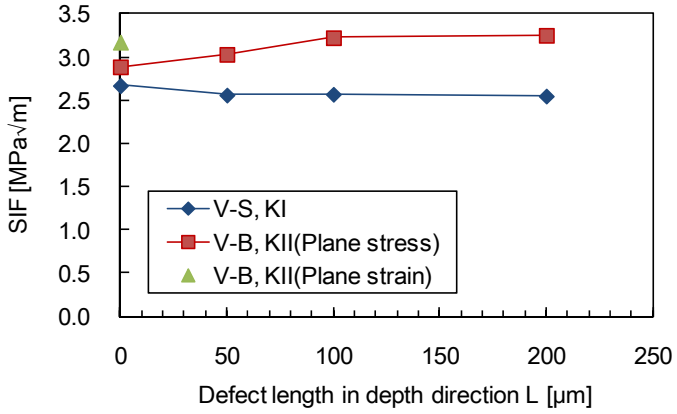

Figure 8: Comparison of ΔK_I at the surface edge of vertical crack and ΔK_{II} at the bottom of vertical crack between different defect lengths (V:vertical crack, S:surface, and B:bottom).

Discussion

Synthesizing the above experimental and analytical results, the authors believe that the degradation of flaking life due to the longer length of defect with the diameter of 15 μm is caused by the following mechanism. Vertical cracks are likely to form at surface edge of defects because a remarkably large tensile residual stress is generated and tension–compression and alternate shear stresses vary widely during rolling contact. Vertical cracks propagate in depth direction along defects, later, when the vertical crack tip reaches the bottom of the defect, the propagation of the vertical crack is retarded. Therefore, longer defects lead to rapid propagation of vertical crack. The authors' previous study [6] revealed that the existence of vertical cracks accelerates the propagation of horizontal cracks causing flaking. Above process implies that longer defects shorten the flaking life. On the other hand, flaking life in the case including a defect with the diameter of 50 μm does not change regardless of the difference of the defect lengths. This is probably because the horizontal cracks form and propagate before vertical cracks grow to the effective size.

Conclusion

RCF test was conducted using specimens with artificial defects which simulate stringer-type inclusions. The effect of defect length on flaking life was evaluated using specimens with different-length defects. The following results were obtained.

(1) In the case of the defect with the 15 μm diameter, flaking life decreased with increasing defect length. In the case of the defect with the 50 μm diameter, flaking life was almost constant from 50 to 300 μm of defect length and shorter than the shortest life in the case of the 15-μm-diameter defect.

(2) In a comparison of the CT image and the SEM view, the shapes of defects and the locations of the horizontal cracks were almost the same respectively, but the shapes of vertical cracks in CT images were smaller in the deeper region than those in SEM views.

(3) Stress states around a circular hole during rolling contact were calculated by elastic-plastic FE analysis. Remarkably high tensile residual stress was generated at the surface edge of the defect. Defects led to higher tensile residual stress than that without defects in the region where the defect exists. The shear stress range at 0.1 mm depth on the middle line of the hole increased with increasing defect length.

(4) The SIFs of the RCF cracks were calculated by elastic FE analysis. The range of mode II SIF ΔK_{II} at the bottom of a vertical crack increased with increasing defect length.

(5) Above analytical results described in (3), (4) provided valuable information for understanding the mechanism of the experimental results described in (1), (2).

Acknowledgements

The synchrotron radiation experiments were performed at BL19B2 in SPring-8 with the approval of the Japan Synchrotron Radiation Research Institute (JASRI) under proposal numbers 2011A1787, 2011B1955, 2012A1596, 2012B1306, and 2013A1307.

References

[1] Chen, Q., Shao, E., Zhao, D., Guo, J., Fan, Z., Measurement of the critical size of inclusions initiating contact fatigue cracks and its application in bearing steel, Wear, 147 (1991) 285–294.

[2] Lewis, M. W. J., Tomkins, B., A fracture mechanics interpretation of rolling bearing fatigue, proceedings of the institution of mechanical engineers, Part J. J Eng. Tribol., 226(5) (2012) 389–405.

[3] Nagao, M., Hiraoka, K., Unigame, Y., Influence of nonmetallic inclusion size on rolling contact fatigue life in bearing steel, Sanyo Tech Report, 12(1) (2005) 38–45 (in Japanese).

[4] Neishi, Y., Makino, T., Matsui, N., Matsumoto, H., Higashida, M., Ambai, H., Influence of the Inclusion Shape on the Rolling Contact Fatigue Life of Carburized Steels, Metall. Mater. Trans. A, 44(5) (2013) 2131–2140.

[5] Nakai, Y., Shiozawa, D., Fukuda, Y., Neishi, Y., Makino, T., Observation of cracks in carbon steel under contact rolling fatigue by micro CT imaging using ultrabright synchrotron radiation, 15th International conference on experimental mechanic, Paper Ref:2635, (2012)

[6] Makino, T., Neishi, Y., Shiozawa, D., Fukuda, Y., Kajiwara, K., Nakai, Y., Evaluation of rolling contact fatigue crack path in high strength steel with artificial defects, Int. J. of Fatigue, 68 (2014) 168-177.